2010 IEEE International Conference on Robotics and Automation
Anchorage Convention District
May 3-8, 2010, Anchorage, Alaska, USA

Desktop Orthogonal-Type Robot with Abilities of Compliant Motion and Stick-Slip Motion for Lapping of LED Lens Molds

Fusaomi Nagata, Takanori Mizobuchi, Shintaro Tani, Tetsuo Hase,
Zenku Haga, Keigo Watanabe, Maki K. Habib and Kazuo Kiguchi

Abstract— **In this paper, a new desktop orthogonal-type robot, which has abilities of compliant motion and stick-slip motion, is first presented for lapping small metallic molds with curved surface. The robot consists of three single-axis devices with a high position resolution of 1μm. A thin wood stick tool is attached to the tip of the z-axis. The tool tip has a small ball-end shape. The control system is composed of a force feedback loop, position feedback loop and position feedforward loop. The force feedback loop controls the polishing force consisting of tool contact force and kinetic friction forces. The position feedback loop controls the position in pick feed direction, e.g., z-direction. The position feedforward loop leads the tool tip along a desired trajectory called cutter location data (CL data). The CL data are generated from the main-processor of a CAM system. The proposed robot realizes a compliant motion required for the surface following control along a spiral path. In order to improve the lapping performance, a small stick-slip motion control strategy is further added to the control system. The small stick-slip motion is orthogonally generated to the direction of the tool moving direction. Generally, the stick-slip motion is an undesirable phenomenon and should be eliminated in precision machineries. However, the proposed robot employs a small stick-slip motion to improve the lapping quality. The effectiveness of the robot is examined through an actual lapping test of an LED lens mold with a diameter of 4 mm.**

I. INTRODUCTION

In manufacturing process of small lens molds such as an LED lens and pickup lens, 3D CAD/CAM systems and NC machining centers are used generally, and these advanced systems have rationalized the design and manufacturing process. However, the lapping process after machining process has been hardly automated yet, because an LED lens mold has plural small concave areas to be finished. That means the target mold is not axis-symmetric. Although almost conventional effective polishing systems can deal with axis-symmetric workpieces but cannot be applied to such an LED lens mold. In other words, no effective finishing systems have been successfully developed for axis-asymmetric LED lens molds. For example, Tsai et al. developed a mold polishing robot [1] and its path planning technique [2], however, the applicability to small axis-asymmetric LED lens molds was not described. Actually, we could not find out other previous literature concerning the finishing of axis-asymmetric LED lens molds. Therefore, as shown in Fig. 1, axis-asymmetric LED lens molds are manually finished by skilled workers in almost cases.

Fig. 1. Hand lapping scene of an LED lens mold.

In this paper, a new desktop orthogonal-type robot, which has abilities of compliant motion and stick-slip motion, is first presented for lapping small metallic molds with curved surface. The robot consists of three single-axis devices with a high position resolution of 1 μm. A thin wood stick tool is attached to the tip of the z-axis. The tool tip has a small ball-end shape. The control system is composed of a force feedback loop, position feedback loop and position feedforward loop. The force feedback loop controls the polishing force consisting of tool contact force and kinetic friction forces. The position feedback loop controls the position in pick feed direction, e.g., z-direction. The position feedforward loop leads the tool tip along a desired trajectory called cutter location data (CL data). The CL data are generated from the main-processor of a CAM system. The proposed robot realizes a compliant motion required for the surface following control along a spiral path.

In order to improve the finishing performance, a small stick-slip motion control strategy is further added to the control system. The small stick-slip motion is orthogonally generated to the direction of the tool moving direction. Generally, the stick-slip motion is an undesirable phenomenon and should be eliminated in precision machineries [3], [4]. However, the proposed robot employs a small stick-slip

F. Nagata, T. Mizobuchi and S. Tani are with the Department of Mechanical Engineering, Faculty of Engineering, Tokyo University of Science, Yamaguchi 756-0884, Japan nagata@ed.yama.tus.ac.jp

T. Hase and Z. Haga are with the R&D Center, Meiho Co. Ltd., Nogata 822-0001, Japan {hase,haga}@meiho-j.co.jp

K. Watanabe is with the Department of Intelligent Mechanical Systems, Graduate School of Natural Science and Technology, Okayama University, Okayama 700-8530, Japan watanabe@sys.okayama-u.ac.jp

Maki K. Habib is with the Mechanical Engineering Department, School of Sciences and Engineering, American University in Cairo, Cairo 11511, Egypt maki@aucegypt.edu

K. Kiguchi is with the Department of Mechanical Engineering, Faculty of Science and Engineering, Saga University, Saga 840-8502, Japan kiguchi@me.saga-u.ac.jp

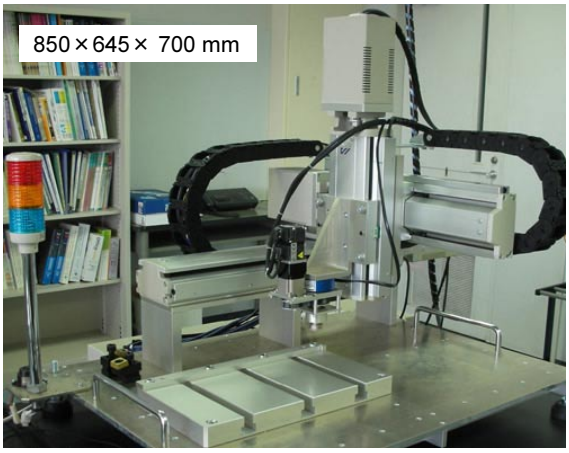

Fig. 2. Proposed desktop orthogonal-type robot with compliance control capability.

motion to improve the lapping quality. The effectiveness of the robot is examined through an actual lapping test of an LED lens mold with a diameter of 4 mm. It is expected that the undesirable small cusps can be uniformly removed and the robot has an effectiveness to achieve a higher quality surface like a mirror finishing due to the abilities of compliant motion and stick-slip motion.

II. DESKTOP ORTHOGONAL-TYPE ROBOT

Figure 2 shows the developed desktop orthogonal-type robot consisting of three single-axis devices with position resolution of 1 μm. The size is 850 $\times$ 645 $\times$ 700 mm. The single-axis device is a position control robot ISPA with high-precision resolution provided by IAI Corp., which is comprised of a base, linear guide, ball-screw, AC servo motor. The effective strokes in x-, y- and z-directions are 400, 300 and 100 mm, respectively. The tool axis is designed to be parallel to z-axis of the robot. A wood stick tool is fixed to the tip through a 3-DOF compact force sensor. To regulate the rotation, a servo spindle is located parallel to the tool axis. The hardware block diagram is shown in Fig. 3. The position resolution and force resolution, and effective stiffness at the tool tip were examined through a simple contact experiment, so that the force resolution of 0.178 N was obtained due to the position resolution of 1 μm. Therefore, the effective stiffness can be estimated as 178 N/mm.

III. COMPLIANT MOTION OF BALL-END ABRASIVE TOOL

A. CAD/CAM-Based Position/Force Control with Weak Coupling

The basic lapping strategy is conducted along a continuous spiral path while performing stable polishing force control. In this section, the control system is explained. The tool tip is controlled by the translational velocity ${}^W\boldsymbol{v}(k) = [{}^W v_x(k)\ {}^W v_y(k)\ {}^W v_z(k)]^T$ given by

$$ {}^W\boldsymbol{v}(k) = {}^W\boldsymbol{v}_t(k) + {}^W\boldsymbol{v}_n(k) + {}^W\boldsymbol{v}_p(k) \tag{1} $$

where k denotes the discrete time; superscript ^{W} denotes the work coordinate system. Note that the control system realized 1 msec sampling time by using the Windows multimedia timer, which was confirmed by using a data logger system. It is assumed that the polishing force is the resultant force of the contact force and kinetic friction forces, and is obtained as the resultant force of x-, y- and z-directional force sensor measurements. Figure 4 shows the proposed CAD/CAM-based position/force controller with weak coupling [5]. First of all, ${}^W\boldsymbol{v}_t(k)$ is the manipulated variable generated from the feedforward control law based on cutter location data called the CL data. ${}^W\boldsymbol{v}_t(k)$ is the tangential velocity and written by

$$ {}^W\boldsymbol{v}_t(k) = v_{tangent}(k)\frac{{}^W\boldsymbol{t}(k)}{\left\|{}^W\boldsymbol{t}(k)\right\|} \tag{2} $$

where $v_{tangent}(k)$ is a velocity scalar. ${}^W\boldsymbol{t}(k)$ is the tangential vector calculated by the CL data.

${}^W\boldsymbol{v}_n(k)$ is the manipulated variable generated from the force feedback control law. ${}^W\boldsymbol{v}_n(k)$ is the normal direction velocity and written by

$$ {}^W\boldsymbol{v}_n(k) = v_{normal}(k){}^W\boldsymbol{o}_d(k) \tag{3} $$

where ${}^W\boldsymbol{o}_d(k)$ is the normalized normal direction vector calculated using the CL data. The scalar $v_{normal}(k)$ representing the normal velocity is the output of the impedance model following force control law [5] given by

$$ \begin{aligned} v_{normal}(k) = {} & v_{normal}(k-1)e^{-\frac{B_d}{M_d}\Delta t} \\ & + \left(e^{-\frac{B_d}{M_d}\Delta t} - 1\right)\frac{K_f}{B_d}E_f(k) \end{aligned} \tag{4} $$

where K_f is the force feedback gain, and impedance parameters M_d and B_d are the desired mass and damping coefficients, respectively. Δt is the sampling time. $E_f(k)$ is the error between the desired polishing force F_d and norm of force ${}^S\boldsymbol{F}(k) \in \Re^3$ measured by the force sensor, which is given by

$$ E_f(k) = F_d - \|{}^S\boldsymbol{F}(k)\| \tag{5} $$

where superscript ^{S} represents the sensor coordinate system. Further, ${}^W\boldsymbol{v}_p(k)$ is the manipulated variable yielded by a position feedback control law given by

$$ {}^W\boldsymbol{v}_p(k) = \boldsymbol{S}_p\Big\{\boldsymbol{K}_p\boldsymbol{E}_p(k) + \boldsymbol{K}_i\sum_{n=1}^{k}\boldsymbol{E}_p(n)\Big\} \tag{6} $$

where the switch matrix $\boldsymbol{S}_p = \mathrm{diag}(S_x, S_y, S_z)$ makes the weak coupling control to the force control active or inactive in each direction; $\boldsymbol{E}_p(k) = {}^W\boldsymbol{x}_d(k) - {}^W\boldsymbol{x}(k)$ is the position error. The desired position ${}^W\boldsymbol{x}_d(k)$ is calculated using CL data. $\boldsymbol{K}_p = \mathrm{diag}(K_{px}, K_{py}, K_{pz})$ and $\boldsymbol{K}_i = \mathrm{diag}(K_{ix}, K_{iy}, K_{iz})$ are proportional and integral gains for position feedback control. Due to the weak coupling control, it is simultaneously realized that stable polishing force control and position control along a spiral path.

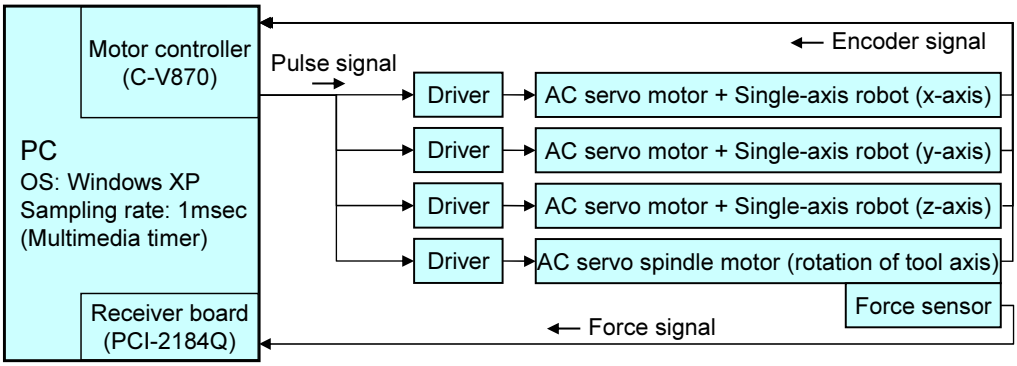

Fig. 3. Hardware block diagram of the proposed robot composed of three single-axis devices with a position resolution of 1μm.

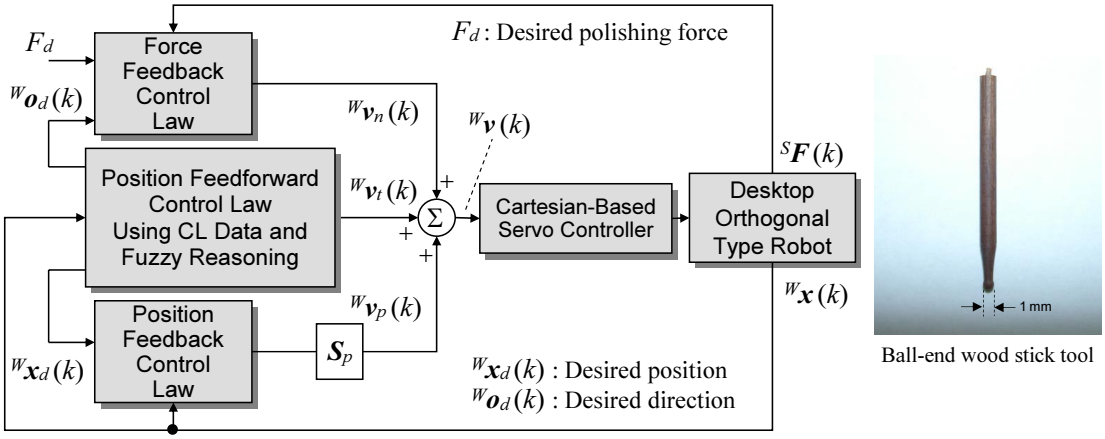

Fig. 4. CAD/CAM-based position/force controller for a ball-end wood stick tool to realize a motion like the desired hand lapping.

B. Tuning of Desired Damping

Next, a tuning method of desired damping is proposed by using the effective stiffness of the robot. When the polishing force is controlled, the characteristics of force control system can be varied according to the combination of impedance parameters such as desired mass and damping. In order to increase the force control stability, the desired damping which has much influence on force control stability should be tuned suitably. In this section, a tuning method of the desired damping is proposed based on the critical damping condition with the effective stiffness of the orthogonal-type robot.

By the way, Eq. (4) is derived from the following impedance model.

$$M_d(\ddot{x} - \ddot{x}_d) + B_d(\dot{x} - \dot{x}_d) = K_f(F - F_d) \tag{7}$$

where $\ddot{x}$, $\dot{x}$ and F are the acceleration, velocity and force scalars in the direction of force control, respectively. $\ddot{x}_d$, $\dot{x}_d$ and F_d are the desired acceleration, velocity and force, respectively. When the force control is active, $\ddot{x}_d$ and $\dot{x}_d$ are set to zero. It is assumed that F is the external force given by the environment and is model as

$$F = -B_m\dot{x} - K_m x \tag{8}$$

where B_m and K_m are the effective viscosity and stiffness coefficients of the system, respectively. Eqs. (7) and (8) lead to the following second order lag system.

$$\ddot{x} + \frac{B_d + K_f B_m}{M_d}\dot{x} + \frac{K_f K_m}{M_d}x = 0 \tag{9}$$

The characteristics equation of Eq. (9) is written by

$$s^2 + \frac{B_d + K_f B_m}{M_d}s + \frac{K_f K_m}{M_d} = 0 \tag{10}$$

In this case, the damping coefficient ζ and natural frequency ω_n are given by

$$\zeta = \frac{B_d + K_f B_m}{2\sqrt{M_d K_f K_m}}, \qquad \omega_n = \sqrt{\frac{K_f K_m}{M_d}} \tag{11}$$

Further, solving Eq. (10) for B_d using the critical damping condition, the following condition is obtained.

$$B_d = 2\sqrt{M_d K_f K_m} - K_f B_m \tag{12}$$

In experiments, the base value for the desired damping is calculated with Eq. (12). The desired damping should be fine-tuned around the base value.

C. Experiment

In this subsection, the proposed robot is applied to the lapping of the LED lens mold. Figure 5 shows the model designed by the 3D CAD/CAM Pro/ENGINEER. The model is designed based on an edge of the mold profile. First of all, an inner edge is drawn in 2D. Then, z-axis is defined as

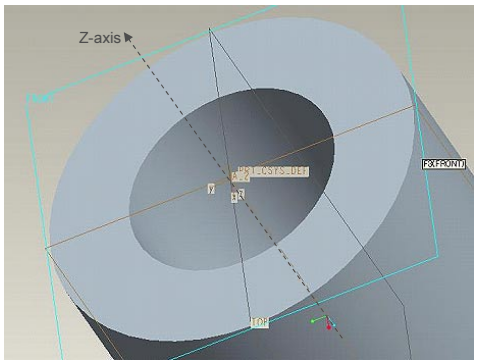

Fig. 5. 3D model of an LED lens mold designed by 3D CAD/CAM Pro/Engineer.

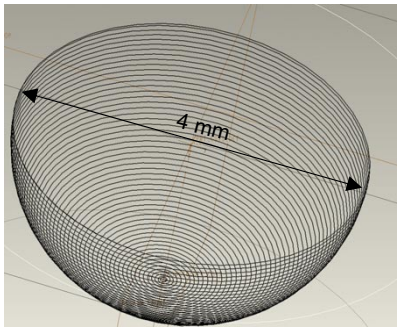

Fig. 6. Spiral path generated by using the main-processor of the CAM, which is used for the desired trajectory of the wood stick tool.

shown in Fig. 5. After that, an inner surface can be created by revolving the edge around the z-axis. Figure 6 shows the spiral path generated from the main-processor of the CAM, which is used in the lapping experiment. The spiral path has sequential position and orientation components.

Figure 7 shows the lapping scene of the LED lens mold, where a special oil including the diamond lapping paste is poured. In this case, a small ball-end tool lathed from a wood stick is used, whose tip diameter is 1 mm. Figure 8 shows the surfaces before and after the lapping process. It is observed that the concaved surface area has a good quality like a mirror surface reflecting the room lights. Although small oily spots are observed, they can be cleaned easily.

IV. STICK-SLIP MOTION OF BALL-END ABRASIVE TOOL

V. STICK-SLIP MOTION CONTROL

In this section, the effectiveness of the tool's stick-slip motion is evaluated to improve the surface quality. Generally, the stick-slip motion is an undesirable phenomenon and should be eliminated in various precise machine tools. However, the proposed orthogonal-type robot employs a small stick-slip motion not only to improve the finishing quality but also to skillfully strengthen the polishing energy. Figure 9 shows the image of the stick-slip motion seen like small vibrations. The stick-slip motion is given along curved surface and also to orthogonal directions of tool tangential velocity ${}^W\boldsymbol{v}_t(k)$. Here, how to generate small

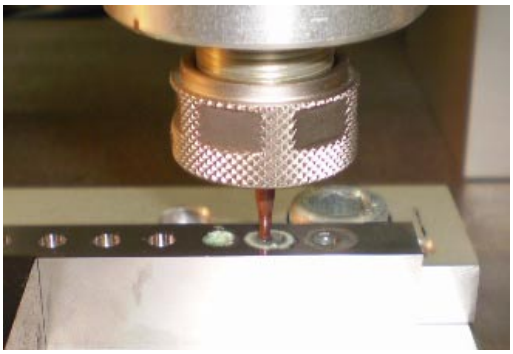

Fig. 7. Lapping scene by using the proposed robot, in which a special oil including diamond lapping paste is poured.

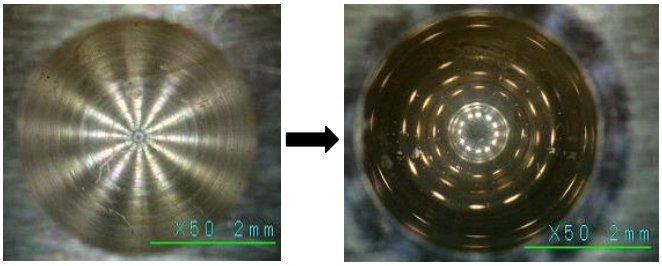

Fig. 8. Finished surface before and after the basic lapping process.

stick-slip motion vectors is explained in detail by using Fig. 10. In Fig. 10, point O is the origin in work coordinate system, where the tool tip initially contacts the workpiece. Point P is the current contact point. ${}^W\boldsymbol{x}(k)$ is the position vector given by ${}^W\boldsymbol{x}(k) = [{}^Wx(k)\ {}^Wy(k)\ {}^Wz(k)]^T$ viewed from O; ${}^W\boldsymbol{o}_d$ is the normalized normal vector at the point P given by ${}^W\boldsymbol{o}_d = [{}^Wo_{dx}(k)\ {}^Wo_{dy}(k)\ {}^Wo_{dz}(k)]$; ${}^W\boldsymbol{t}(k) = [{}^Wt_x(k)\ {}^Wt_y(k)\ {}^Wt_z(k)]^T$ is the tangential vector at the point P. Here, it is assumed that ${}^W\boldsymbol{v}_v(k) = [{}^Wv_{vx}(k)\ {}^Wv_{vy}(k)\ {}^Wv_{vz}(k)]^T$ is a small stick-slip motion vector.

In this example, the tool approaches to the workpiece with a low speed and follow the spiral path after contacting the point O. Because ${}^W\boldsymbol{v}_v(k)$ is perpendicular to ${}^W\boldsymbol{o}_d(k)$, the following relation is obtained.

$$ {}^Wv_{vx}(k)\ {}^Wo_{dx}(k) + {}^Wv_{vy}(k)\ {}^Wo_{dy}(k) + {}^Wv_{vz}(k)\ {}^Wo_{dz}(k) = 0 \tag{13} $$

Also, ${}^W\boldsymbol{v}_v(k)$ and ${}^W\boldsymbol{t}(k)$ are orthogonal each other, so that

$$ {}^Wv_{vx}(k)\ {}^Wt_x(k) + {}^Wv_{vy}(k)\ {}^Wt_y(k) + {}^Wv_{vz}(k)\ {}^Wt_z(k) = 0 \tag{14} $$

Further, ${}^W\boldsymbol{v}_v(k)$ is located in a plane which includes both ${}^W\boldsymbol{o}_d(k)$ and ${}^W\boldsymbol{x}(k)$, so that the components of ${}^W\boldsymbol{v}_v(k)$ are represented by

$$ {}^Wv_{vx}(k) = i\ {}^Wo_{dx}(k) + j\ {}^Wx(k) \tag{15} $$

$$ {}^Wv_{vy}(k) = i\ {}^Wo_{dy}(k) + j\ {}^Wy(k) \tag{16} $$

$$ {}^Wv_{vz}(k) = i\ {}^Wo_{dz}(k) + j\ {}^Wz(k) \tag{17} $$

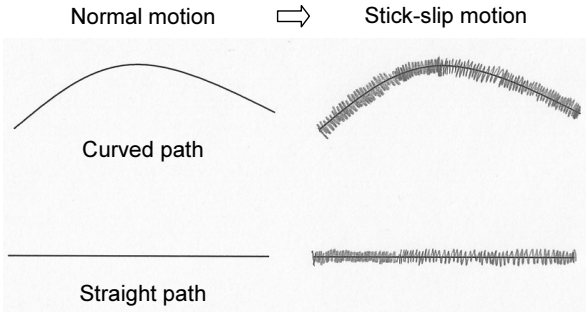

Fig. 9. Image of the small stick-slip motion seen like small vibrations for an abrasive tool.

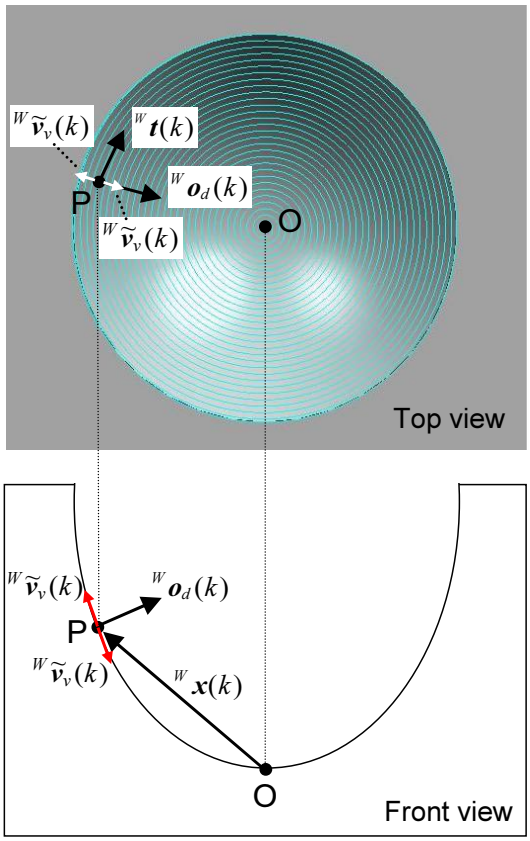

Fig. 10. Theoretical idea to calculate the stick-slip motion vector ${}^W\boldsymbol{v}_v(k)$, where the directions of ${}^W\boldsymbol{v}_t(k)$ and ${}^W\boldsymbol{v}_n(k)$ are the same ones of ${}^W\boldsymbol{t}(k)$ and ${}^W\boldsymbol{o}_d(k)$, respectively.

where i and j are real numbers. By solving the Eqs. (13), (14), (15), (16) and (17), ${}^W v_{vx}(k)$, ${}^W v_{vy}(k)$ and ${}^W v_{vz}(k)$ can be obtained. Here, however, a simpler calculation is used. First of all, substituting Eqs. (15), (16) and (17) into Eq. (13) and considering $\|{}^W\boldsymbol{o}_d(k)\|$=1 lead to

$$i = -j\{{}^W o_{dx}(k)\ {}^W x(k) + {}^W o_{dy}(k)\ {}^W y(k) + {}^W o_{dz}(k)\ {}^W z(k)\} \quad (18)$$

Accordingly, by giving Eq. (18) into Eqs. (15), (16) and (17), the following equations are obtained.

$$\begin{aligned} {}^W v_{vx}(k) = j\{&{}^W x(k) - ({}^W o_{dx}(k)\ {}^W x(k) \\ &+ {}^W o_{dy}(k)\ {}^W y(k) + {}^W o_{dz}(k)\ {}^W z(k))\ {}^W o_{dx}(k)\} \end{aligned} \quad (19)$$

$$\begin{aligned} {}^W v_{vy}(k) = j\{&{}^W y(k) - ({}^W o_{dx}(k)\ {}^W x(k) \\ &+ {}^W o_{dy}(k)\ {}^W y(k) + {}^W o_{dz}(k)\ {}^W z(k))\ {}^W o_{dy}(k)\} \end{aligned} \quad (20)$$

$$\begin{aligned} {}^W v_{vz}(k) = j\{&{}^W z(k) - ({}^W o_{dx}(k)\ {}^W x(k) \\ &+ {}^W o_{dy}(k)\ {}^W y(k) + {}^W o_{dz}(k)\ {}^W z(k))\ {}^W o_{dz}(k)\} \end{aligned} \quad (21)$$

Because both ${}^W\boldsymbol{o}_d(k)$ and ${}^W\boldsymbol{x}(k)$ are known, ${}^W\boldsymbol{v}_v(k)$ can be normalized as $\boldsymbol{v}_v(k)/\|\boldsymbol{v}_v(k)\|$. Further, by using a gain K_v and a sign SIGN(k), the stick-slip motion vector is finally obtained as

$${}^W\tilde{\boldsymbol{v}}_v(k) = \text{SIGN}(k)\ K_v\ \frac{\boldsymbol{v}_v(k)}{\|\boldsymbol{v}_v(k)\|} \quad (22)$$

where SIGN(k) is given by

$$\text{SIGN}(k) = \begin{cases} 1 & \text{if } k = \text{odd number} \\ -1 & \text{otherwise} \end{cases} \quad (23)$$

${}^W\tilde{\boldsymbol{v}}_v(k)$ is a velocity vector to yield another polishing energy, and which is given to the tool alternately changing the direction every sampling period. Figure 11 shows the block diagram of the controller with the stick-slip motion control method. As can be seen from Eqs. (2) and (3), the directions of ${}^W\boldsymbol{v}_t(k)$ and ${}^W\boldsymbol{v}_n(k)$ are the same ones of ${}^W\boldsymbol{t}(k)$ and ${}^W\boldsymbol{o}_d(k)$, respectively. Also, ${}^W\boldsymbol{v}_p(k)$ is generated in the direction of z-axis as shown in Fig. 5 called the spiral direction.

It should be noted that the total finishing time depends on the tangential velocity ${}^W\boldsymbol{v}_t(k)$, so that there is no time difference between the cases with and without using the stick-slip motion.

A. Experiment of Stick-Slip Motion

Next, the effectiveness of the stick-slip motion control is examined through an actual lapping test. In the conventional lapping method shown in Fig. 4, the proposed stick-slip motion was not applied. Although the concaved area after the lapping process shown in Fig. 8 may be seen as a high quality surface, uneven lines are observed as shown in Fig. 12, in which small cusps still remain. On the other hand, Fig. 13 shows the large scale photo of the LED lens mold after the lapping process by using the proposed stick-slip motion control as shown in Fig. 11. It is observed that the undesirable cusps can be almost removed uniformly. In this case, the gain K_v to regulate the amplitude is empirically set to 10, so that the amplitude $\|{}^W\tilde{\boldsymbol{v}}_v(k)\|$ can be estimated 10 μm.

It has been confirmed from the result that the proposed lapping strategy by using the stick-slip motion control has an effectiveness to achieve a higher quality surface. It is not easy to measure the quantitative value on surface roughness of concavely machined small area, so that a special 3D measurement system is being considered.

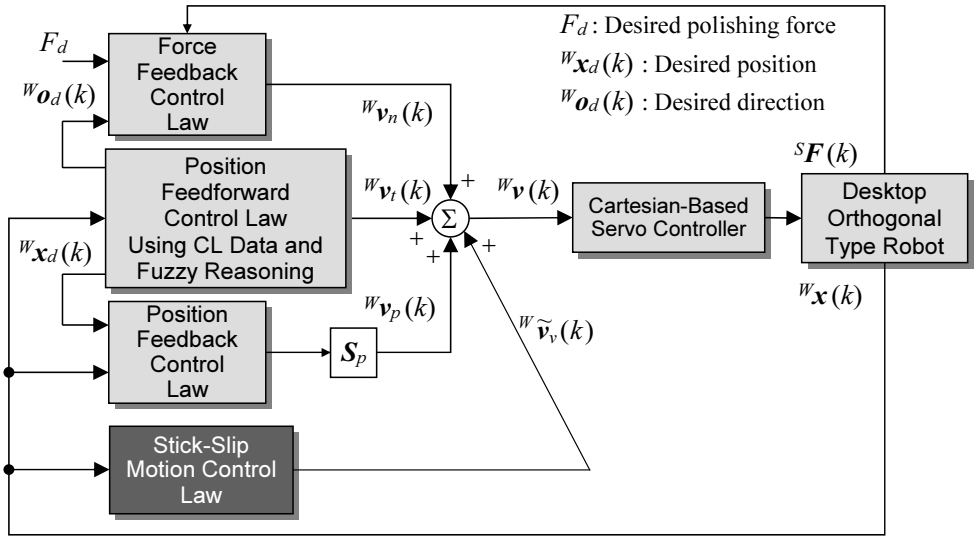

Fig. 11. CAD/CAM-based position/force controller with the proposed stick-slip motion.

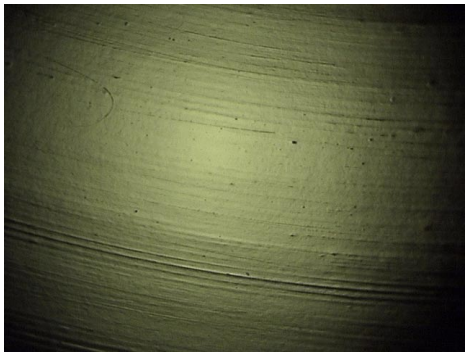

Fig. 12. Large scale photo of the LED lens mold, where undesirable small cusps still remained on the surface.

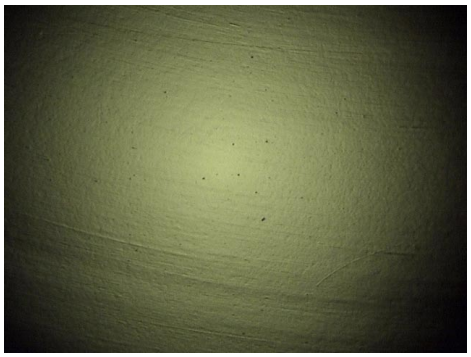

Fig. 13. Large scale photo of the LED lens mold after the lapping process by using the proposed stick-slip motion control.

VI. CONCLUSIONS

The final goal of this study is the development of a novel orthogonal-type robot with compliance controllability that can be applied to from the cusp mark removing process to the finishing process for mirror-like surface of LED lens molds. In this paper, a desktop orthogonal-type robot was first designed by combining three single-axis devices. The position resolution and force resolution, and effective stiffness were examined through a simple contact experiment, so that the force resolution of 0.083 N was obtained due to the position resolution of 1 μm. Next, the CAD/CAM-based position/force controller with compliance controllability was proposed for the lapping task of LED lens molds, in which position control, force control or their weak coupling control can be selected according to each finishing strategy. A systematic tuning method of the desired damping was also considered. The desired damping was calculated from the critically damped condition using the static relation between the position and force. Further, a stick-slip motion control for a wood stick tool was developed to skillfully improve the finishing quality. The proposed desktop orthogonal-type robot using these peripheral techniques was applied to a lapping experiment of an LED lens mold, so that the high performance and promise were successfully confirmed. In future work, we plan to develop an automated tool truing system for continuously lapping plural LED lens molds so that the proposed robot can be used in actual manufacturing fields.

VII. ACKNOWLEDGMENTS

This work was partly supported by Grant-in-Aid for Scientific Research (C) (20560248).

REFERENCES

[1] M.J. Tsai, J.L. Chang and J.F. Haung, "Development of an Automatic Mold Polishing System, " *Procs. of 2003 IEEE Int. Conf. on Robotics & Automation*, pp. 3517–3522, Taipei, Taiwan, 2003.

[2] M.J. Tsai, J.J. Fang and J.L. Chang, "Robotic Path Planning for an Automatic Mold Polishing System, *International Journal of Robotics and Automation*, vol. 19, no. 2, pp. 81–89, 2004.

[3] O. Bilkay and O. Anlagan, "Computer Simulation of Stick-Slip Motion in Machine Tool Slideways," *Tribology International*, vol. 37, no. 4, pp. 347–351, 2004.

[4] X. Mei, M. Tsutsumi, T. Tao and N. Sun, "Study on the Compensation of Error by Stick-Slip for High-Precision Table," *International Journal of Machine tools & Manufacture*, vol. 44, no. 5, pp. 503–510, 2004.

[5] F. Nagata, T. Hase, Z. Haga, M. Omoto and K. Watanabe, "CAD/CAM-Based Position/Force Controller for a Mold Polishing Robot," *Mechatronics*, vol. 17, no. 4–5, pp. 207–216, 2007.